ac Stark shifts in Rydberg NO levels induced by intense laser pulses

R. B. López-Martens, T. W. Schmidt, and G. Roberts

Department of Chemistry, University of Cambridge, Lensfield Road, Cambridge CB2 1EW, England
(Received 3 January 2000; published 16 June 2000)

We report a quantitative assessment of the ac Stark effect induced in the NO $3s\sigma\ A\ ^2\Sigma^+$ Rydberg state by femtosecond laser pulses at intensities up to $I \lesssim 6 \times 10^{13}\,\mathrm{W\,cm^{-2}}$. The $n' = 2$ vibrational level of $A\ ^2\Sigma^+$ NO is excited by two-photon absorption at frequencies above and below the weak-field $A\ ^2\Sigma^+ \leftarrow X\ ^2\Pi_r + 2\hbar\omega$ resonance and its time-dependent population monitored by fluorescence detection at different incident laser intensities. Dispersed $A\ ^2\Sigma^+ \rightarrow X\ ^2\Pi_r$ spectra recorded at $I \gtrsim 10^{13}\,\mathrm{W\,cm^{-2}}$ exhibit prominent features due to fluorescence from the $n' = 2$, 1, and 0 levels of the $A\ ^2\Sigma^+$ state. These results can be quantitatively described by a kinetic treatment of multiphoton absorption and ionization that takes into account ac Stark shifting of the vibrational levels of the $A\ ^2\Sigma^+$ state at different coordinates in space time mapped out by the laser pulse. An analysis of the experimental data within the terms of this model leads to the deduction that the ac Stark shift is 0.4 times the ponderomotive energy of a free electron at the laser fields used, corresponding to a shift of 0.36 eV at an intensity of $I = 6 \times 10^{13}\,\mathrm{W\,cm^{-2}}$ at $\lambda = 400$ nm.

PACS number(s): 42.50.Hz, 33.80.Rv, 32.80.Rm, 32.60.+i

I. INTRODUCTION

Much effort has been dedicated to the investigation of the intensity dependence of atomic and molecular energy levels in intense laser fields [1]. In general, the polarizability induced by an optical field shifts all energy levels to some degree, either through Thomson scattering or the ac (dynamical) Stark effect. According to perturbation theory, the energy eigenvalues of a multilevel system bathed in an oscillating electric field E are shifted by the ac Stark effect by an amount [2–4]

$$\epsilon = -\tfrac{1}{4}\alpha(\omega)E^2, \tag{1}$$

where $\alpha(\omega)$ is the induced polarizability and E is the electric vector of the incident light of frequency ω time averaged over a single optical cycle. In particular, the ponderomotive shifting of ionization potentials and high-lying atomic or molecular levels has been discussed [5] to explain photoelectron energy spectra at high laser intensities where above-threshold ionization predominates [6]. From a classical perspective, the ponderomotive energy, $U_p = e^2 E^2/4m\omega^2$, is simply the mean ''wiggle'' energy imparted to a free electron by an oscillating radiation field $E = E_0 \cos(\omega t)$, and is a linear function of intensity I. ac Stark shifts essentially identical to the ponderomotive energy are observed for highly excited atomic states lying close to the ionization limit [7]. For strongly bound states, however, from which the energy of any transition is large compared to the photon energy of the incident field, the excess energy gained due to residual wiggle is much less than U_p. States that lie at intermediate energies between the ground state and the ionization limit undergo Stark shifts whose magnitude and sign depend upon the details of their couplings to neighboring levels induced by the optical field. In particular, the shift of lower-lying Rydberg or valence states in molecules might be expected to differ quite significantly from the ponderomotive energy,

since the induced polarizability strongly depends on the internuclear distance, and hence on the nature of the electronic potential-energy surface [1].

Although many elegant experiments have been designed to determine ponderomotive energy shifts in atomic systems [7], there exist in the literature relatively fewer quantitative determinations of the extent of ac Stark shifting of molecular excited states. Most information on the ac Stark effect in excited electronic states of molecules derives from measurements of line shifts, broadenings, and splittings (the Autler-Townes effect) in frequency-domain measurements carried out at high spectral resolution. Line shifts have been observed in resonant ionization schemes involving the E, $F\ ^1\Sigma_g^+$ state of H_2 [8] and have been utilized to determine the vibronic transition moment between the E, $F\ ^1\Sigma_g^+$ and $D\ ^1\Pi_u$ states [9]. In a similar vein, dynamic Stark shifts in the two-photon resonantly enhanced multiphoton ionization (REMPI) spectrum of vibrational bands of the $A\ ^1\Pi \leftarrow X\ ^1\Sigma^+$ transition of CO have been examined by several groups [10,11], and sub-Doppler spectroscopy has been applied to examine light shifts of the $B\ ^1\Sigma^+\ n' = 0 \leftarrow X\ ^1\Sigma^+\ n'' = 0$ two-photon transition of the same molecule [12]. Girard *et al.* have examined the polarization dependence of the ac Stark effect in the $2+2$ REMPI $a\ ^1\Pi_g \leftarrow X\ ^1\Sigma_g^+$ spectrum of N_2 [11]. The force due to the nonresonant polarizability [Eq. (1)] induced by intense infrared photons has been exploited to modify the trajectory of a beam of CS_2 molecules [13]. Transient resonances induced by ac Stark shifting have been invoked to explain atomic fragment kinetic-energy partitioning in intense-laser dissociation and ionization of $H_2\ B\ ^1\Sigma_u^+\ n = 3$ rotational levels [14] and the five-photon photofragment spectrum of Cl_2 nonresonantly excited via the $3\ ^3\Pi_u$ Rydberg state [15]. The kinetic energy of photoelectrons in Cl_2 dissociative ionization [15] and their angular distribution in $1+1$ resonant autoionization of H_2 $1\sigma_u^2$ [16] at $I \simeq 10^{12}\,\mathrm{W\,cm^{-2}}$ also exhibit characteristics due to dynamical Stark shifting of states. The ac Stark shift of neutral excited states and the ionization potential has been

observed to play an important role in the mechanism of high-harmonic generation in N_2 [17], while the different behavior of Rydberg and valence states in intense laser fields serves to rationalize the structure of N_2 photoelectron spectra in the multiphoton ionization regime [18]. Insightful discussions of theoretical aspects of dynamic Stark shifting of resonant Rydberg states in two-color multiphoton ionization have been given by, among others, l'Huillier *et al.* [19] and Gibson *et al.* [20].

For NO, substantial Stark shifting of spectral lines of the $D\ ^2\Sigma^+\leftarrow X\ ^2\Sigma^+$ transitions at 7 GW cm^{-2} incident intensity has been invoked to explain the spectral width and asymmetry of a laser-dressed continuum structure in $2+1$ ionization that resonantly accesses levels of the dressed $D\ ^2\Sigma^+$ state [21]. Stark broadening of the two-photon $A\ ^2\Sigma^+\ n'=0$ $\leftarrow X\ ^2\Pi_r n''=0$ spectrum induced by 5-ns, 3–GW cm^{-2} laser pulses enabled Huo *et al.* to determine Stark shifts of up to 6.24×10^{-4} eV for rotational components of the Rydberg $A\ ^2\Sigma^+\ n'=0$ level [22]. Shifts of this magnitude, which are larger than the free-electron ponderomotive energy for these laser fields, were attributed by these workers to optical coupling via the Stark field to higher-lying electronic states. The pressure dependence of the ac Stark effect in NO $A\ ^2\Sigma^+$ at GW cm^{-2} intensities has been thoroughly investigated through measurements of asymmetrically broadened line shapes in laser-induced fluorescence and resonant multiphoton ionization spectra [23]. At intensities in the range $\simeq0.8$–20×10^{12} W cm^{-2} at a given wavelength, Ludowise *et al.* observed preferential population of the $C\ ^2\Pi\ n=0$ and $A\ ^2\Sigma^+\ n=3$ vibrational levels of NO by femtosecond photoelectron spectroscopy [24]. These workers estimated a maximum energy shift for the $A\ ^2\Sigma^+$ state of 200 meV at $I=1.6\times10^{13}$ W cm^{-2}, which is within 10% of the full ponderomotive expectation.

The totally nonresonant four-photon ionization of NO in intense 532-nm nanosecond and picosecond pulses has been successfully described by He and Becker [25] using a rate equation model based on perturbation theory. At intensities up to $\simeq2\times10^{13}$ W cm^{-2}, the ionization rate was found to exhibit the characteristic power-law dependence on I of the form

$$\Gamma_{\text{ion}}=\sigma_m I^m,\qquad(2)$$

where σ_m is the total ionization cross section and $m=4$. For pumping at wavelengths such as 532 nm, where the photon energy is far removed from the energies of real states of NO whose occupation would be permitted by selection rules, σ_m remains insensitive to intensity, and a perturbative treatment that does not involve intensity-dependent intermediate energy levels adequately describes the ionization process. However, if the laser wavelength can access a real excited state with an intermediate number of photons, such a state may be shifted into and out of resonance by the time-varying laser intensity. These transient resonances will affect the time-dependent population dynamics of the intermediate excited state and thus any subsequent process that depends on them, whether it be ionization during the remainder of the
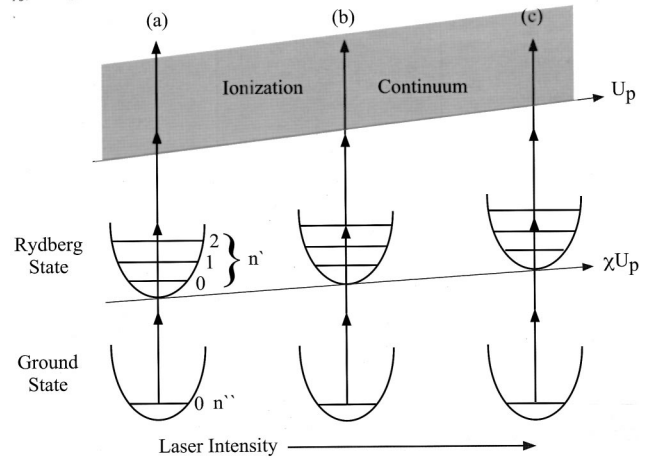

FIG. 1. Schematic illustration of the interaction of intense laser light with NO, showing the upward shifting of the ionization threshold and the $A\ ^2\Sigma^+$ Rydberg state induced by the electric field of the laser as its intensity increases during the first half of the pulse: the ionization threshold increases by an amount equivalent to the free-electron ponderomotive energy U_p; the ac Stark effect in NO $A\ ^2\Sigma^+$ is governed by optical coupling of the $A\ ^2\Sigma^+$ state to other Rydberg and valence states of the molecule mediated by the stark field, and is expressed as a fraction χ ($0\le\chi\le1$) of U_p. The intense optical field distorts the potential-energy curves and the ground state also experiences a small ac Stark effect, neither of which are shown. The length of the vertical arrows represents photon energies for two-photon $A\ ^2\Sigma^+\leftarrow X\ ^2\Pi_r$ absorption at $\lambda=400$ nm, showing above-resonance $n'=2\leftarrow n''=0$ excitation at the lowest intensity (a), resonant $n'=2\leftarrow n''=0$ excitation at the middle intensity (b), and below-resonant $n'=2\leftarrow n''=0$ excitation at the highest intensity.

pulse or fluorescence from the excited state once the molecule has left the focal volume of the laser.

In this paper we present measurements of NO $A\ ^2\Sigma^+$ $\rightarrow X\ ^2\Pi_r$ fluorescence induced by a femtosecond laser as a function of intensity up to $\simeq6\times10^{13}$ W cm^{-2} and photon energies scanned from nonresonantly below to nonresonantly above that for the NO $A\ ^2\Sigma^+\ n'=2\leftarrow X\ ^2\Pi_r n''=0$ two-photon transition in the weak-field limit. Figure 1 illustrates, in cartoon fashion, the nature of our experiment. The $A\ ^2\Sigma^+$ state of NO corresponds to a single electron occupying the atomiclike $3s\sigma$ orbital. Although labeled as a Rydberg state and characterized by a Coulombic attractive force, the $A\ ^2\Sigma^+$ state lies at an intermediate energy, approximately 5.49 eV above the ground state and 3.77 eV below the ionization threshold situated at 9.26 eV [26]. It cannot be assumed *a priori* that, in an intense laser field, the ac Stark shift for this state will be fully ponderomotive, and thus it is of interest to seek to quantify this energy shift as accurately as possible, and compare it to the ponderomotive energy of a free electron.

As Fig. 1 attempts to convey, the onset for resonant population of the $A\ ^2\Sigma^+\ n'=2$ Rydberg vibrational level, and subsequent $A\ ^2\Sigma^+\ n'=2\rightarrow X\ ^2\Pi_r n''=0$ fluorescence, is observed at progressively higher laser intensities as the excitation wavelength is decreased to the blue of the weak-field limit of the two-photon transition. The dependence of

$A\ ^2\Sigma^+\ n'=2\rightarrow X\ ^2\Pi_r\ n''=0$ fluorescence on laser intensity is mimicked for intensities up to $\simeq 2.5\times 10^{13}\,\mathrm{W\,cm^{-2}}$ by solving kinetic rate equations for the time-dependent populations in the ground state and the three lowest vibrational levels of the $A\ ^2\Sigma^+$ state of NO. Stark tuning of the $A\ ^2\Sigma^+$ vibrational levels into resonance at different intensities is accounted for by rendering the two-photon $A\ ^2\Sigma^+\leftarrow X\ ^2\Pi_r$ absorption cross section intensity-dependent, whereby the ''resonant'' transition energy shifts linearly with laser intensity. The usefulness of the kinetic approach is discussed in terms of its ability to predict the magnitude of the ac Stark shift of NO $A\ ^2\Sigma^+$ in comparison to the ponderomotive energy in the same laser field.

II. EXPERIMENT

Ultrafast laser pulses were generated by a regeneratively amplified Ti:sapphire laser (Spectra-Physics Lasers) operating at 10 Hz. Pulse widths were determined by second-order interferometric autocorrelation, from which the (Gaussian) pulse duration was conservatively estimated as $140\pm 10\,\mathrm{fs}$. The compressed output was optimized for emission at regular intervals between 790 and 830 nm such that the peak wavelength of the frequency doubled pulses could be scanned through the NO $A\ ^2\Sigma^+\ n'=2\leftarrow X\ ^2\Pi_r\ n''=0$ two-photon absorption at 409.9 nm [27]. Second-harmonic generation (SHG) was performed in a 1.4-mm potassium dihydrogen phosphate (KDP) crystal cut for type-I SHG at 800 nm. The second-harmonic pulses were focused by a thin fused silica lens (focal length 0.2 m) into a quartz static cell containing approximately 1.6 Torr of NO. The pressure of NO in the cell was chosen to ensure a maximum fluorescence signal without significantly reducing the fluorescence lifetime by vibrational quenching [27]. NO $A\ ^2\Sigma^+\rightarrow X\ ^2\Pi_r$ fluorescence was dispersed in a monochromator and detected photoelectrically perpendicular to the laser propagation axis. Time-resolved fluorescence profiles were displayed and averaged over 100 individual laser shots on a digital oscilloscope and then downloaded onto a laboratory computer and integrated to obtain the total fluorescence at each excitation wavelength. Scans of the dispersed fluorescence at high pump intensities ($I\geqslant 10^{13}\,\mathrm{W\,cm^{-2}}$) revealed a congestion in the fluorescence spectrum due to laser-induced shifting of the $n'=1$ and $n'=0$ vibrational levels of the $A\ ^2\Sigma^+$ state into resonance with the two-photon transition energy. The origins for fluorescence from the $n'=1$ and $n'=0$ levels are situated at 215 and 226 nm, respectively [27]. The detection wavelength was therefore fixed at 205 nm, corresponding to the origin of the NO $A\ ^2\Sigma^+\ n'=2\rightarrow X\ ^2\Pi_r\ n''=0$ transition, with a 5-nm detection bandpass. In this way, the incident intensity dependence of fluorescence from NO $A\ ^2\Sigma^+\ n'=2$ could be monitored in the absence of significant contributions to the total fluorescence signal from the neighboring $A\ ^2\Sigma^+\ n'=1,0\rightarrow X\ ^2\Pi_r\ n''=0$ lines. Fluorescence was recorded as a function of second-harmonic intensity at five different excitation wavelengths encompassing the two-photon $A\ ^2\Sigma^+\ n'=2\leftarrow X\ ^2\Pi_r\ n''=0$ weak-field resonance, as depicted in Fig. 1.

For each set of measurements at a given wavelength, the peak intensity of the excitation pulse was varied by rotating the polarization sense of the fundamental beam prior to the KDP crystal, thus reducing the efficiency of the frequency doubling process and decreasing the output energy of the second-harmonic pulses. The energy of the second-harmonic laser pulses incident on the cell window was monitored by a pyroelectric detector immediately before and after fluorescence collection and could be varied from zero to a maximum of 150 μJ. The second-harmonic pulse energy varied quadratically with input pulse energy accross the entire intensity range used in these experiments, implying that SHG was not saturated and ensuring that the frequency doubled pulses were neither spatially nor temporally distorted as their energy was increased. This allowed us to assume the same spatiotemporal profiles for the second-harmonic pulses throughout the course of measurements at different intensities at a given wavelength, and then for each excitation wavelength.

To ensure an accurate determination of the pulse intensity at each wavelength, a detailed characterization of the laser pulse profiles in space time was carried out. Temporal characterization was performed by mixing the output SHG pulses with a fraction of the fundamental pulse in a beta-barium borate (BBO) crystal of thickness 0.1 mm to generate the third harmonic. Cross-correlation widths varied very little with excitation wavelength and typical values measured before and after each experiment were around 180 fs, implying a second-harmonic pulse width of about 100 fs. Spatial characterization was performed by appropriately attenuating the excitation pulse prior to focus, and directing the laser beam into a charge-coupled-device (CCD) camera placed at the focal point of the lens used in the experiment. The resulting images were captured by a frame grabber and stored on a computer through video image processing software. Typical beam profiles were elliptical in shape with Gaussian intensity profiles along the major and minor axes. For two-photon excitation at 415, 410, 405, and 395 nm, the spatial beam shapes were fitted individually with a minor full width at half maximum (FWHM) of about 30 μm and a major FWHM of 130μm. The 400-nm beam was seen to have a much tighter focus, with dimensions of $30\times 85\ \mu$m. The maximum peak intensity for the 400-nm data was thus much larger than that for the other wavelengths.

At the beam focus, the transverse component corresponding to the minor axis of the elliptical beam profile has the smallest waist size and consequently the smallest and most limiting confocal parameter along the laser propagation axis. For a laser beam with a Gaussian spatial distribution, this waist size corresponds to a confocal distance of approximately 10 mm at $\lambda = 400\,\mathrm{nm}$. Fluorescent emission located about the laser focus was collimated and imaged onto a 1.2-mm entrance slit of the monochromator using a 1:3 lens telescope arrangement. In this way, the only fluorescence collected was that emitted from molecules located within a spatial extent of $\simeq 350\ \mu$m along the laser propagation axis around the position of the minimum beam waist, corresponding to a small fraction of the smallest confocal distance of the laser. Under these conditions, the transverse beam profile varies very little across the spatial region imaged onto the
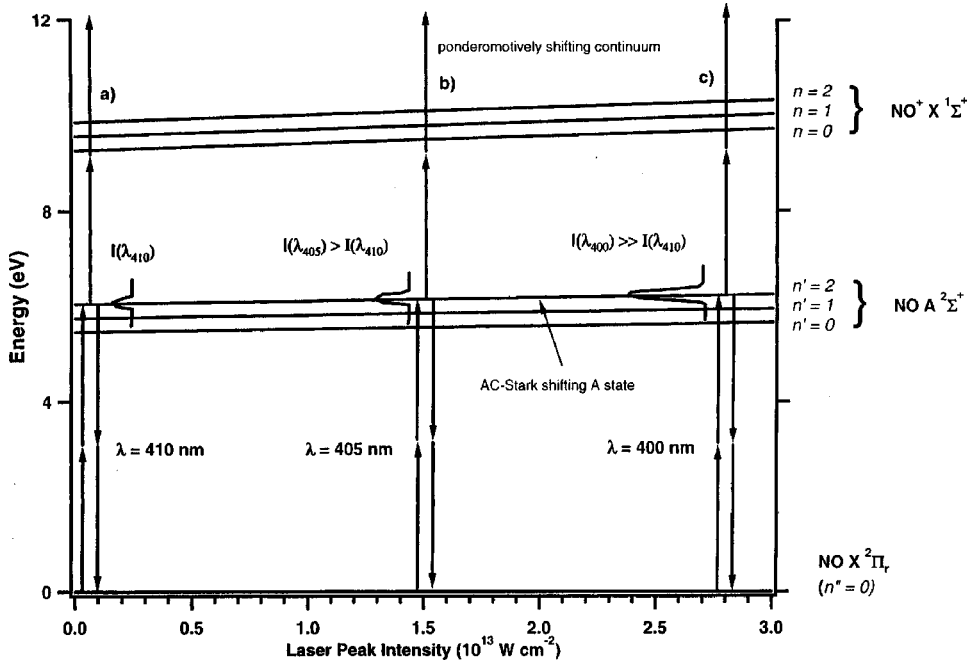
FIG. 2. Energy-level diagram showing the diverse NO multiphoton sequences included in a kinetic simulation of the dependence of $A\ ^2\Sigma^+ \to X\ ^2\Pi_r$ fluoresence on incident laser intensity at $I \lesssim 3 \times 10^{13}\ \mathrm{W\,cm}^{-2}$ and $\lambda = 395$–415 nm. On this energy scale, the induced ac Stark shifts of the NO $A\ ^2\Sigma^+$ state and NO^+ $X\ ^1\Sigma^+$ ground-state vibrational levels are barely discernible: the effect is shown schematically in Fig. 1.

monochromator, thereby generating a constant spatial intensity distribution for the incident radiation along the propagation axis. The total fluorescence collected is therefore an average, assuming a constant transverse beam profile, of the light emitted over the extent along the z axis that is imaged onto the entrance slit of the monochromator.

III. KINETIC MODEL

In this section we present a kinetic scheme for simulating the $A\ ^2\Sigma^+\ n'=2 \to X\ ^2\Pi_r\ n''=0$ fluorescence intensity emitted by NO as a function of incident laser intensity. The model is based on a perturbative description of $2+2$ resonant multiphoton ionization via the $A\ ^2\Sigma^+$ state, using transition cross sections derived in the weak-field limit. The standard perturbation theory result for the rate of depopulation of a state by an mth order process is

$$-\frac{dN}{dt} = N\sigma_m(\omega)\Phi(\omega)^m, \tag{3}$$

where σ_m is the m-photon cross section in units of length^{2m} time^{m-1} and $\Phi(\omega)$ is the photon flux expressed as per unit area per unit time. This type of model has found wide application in studies of multiphoton ionization of atoms [28], and has been adapted previously [25] to model multiphoton transitions in NO up to the intensities employed in the present experiment when all important radiative processes are taken into account: specifically included here are two-photon $A\ ^2\Sigma^+ \leftarrow X\ ^2\Pi_r$ absorption and $A\ ^2\Sigma^+ \to X\ ^2\Pi_r$ stimulated emission, two-photon NO^+ $X\ ^1\Sigma^+ \leftarrow \mathrm{NO}\ A\ ^2\Sigma^+$ ionization and direct NO^+ $X\ ^1\Sigma^+ \leftarrow \mathrm{NO}$ $X\ ^2\Pi_r$ four-photon ionization from the neutral ground state. The last of these processes must be included in any treatment of nonresonant excitation when no vibrational level of the $A\ ^2\Sigma^+$ state is encompassed within the bandwidth of the

ultrashort laser pulse at the two-photon center frequency. Figure 2 displays the intensity-dependent energy levels and optical transitions invoked to model intense laser excitation of NO at $\lambda = 395$–415 nm.

To take account of ac Stark shifting of NO $A\ ^2\Sigma^+$ vibrational levels, coupled differential equations are proposed that include intensity-dependent excitation cross sections, and the state shifting is assumed to be directly proportional to light intensity, as in the ponderomotive shift of a free electron. The kinetic evolution of the populations $N_X(0)$ of the $n'' = 0$ vibrational level of the lower $X\ ^2\Pi_{1/2}$ spin-orbit state of the electronic ground state and $N_{A(n')}$ of the n'th vibrational level of the $A\ ^2\Sigma^+$ state are

$$-\frac{dN_{X(0)}}{dt} = \int dx \int dy$$
$$\times \Bigg\{ \sum_{n'} [N_{X(0)}\sigma^{(2)}_{n'-0}(\omega,\Phi)\Phi(x,y,z;\omega;t)^2$$
$$- 2N_{A(n')}\sigma^{(2)}_{n'-0}(\omega,\Phi)\Phi(x,y,z;\omega;t)^2]$$
$$+ N_{X(0)}\sigma^{(4)}_{\mathrm{ion}-0}\Phi(x,y,z;\omega;t)^4 \Bigg\} \tag{4}$$

and

$$\frac{dN_{A(n')}}{dt} = \int dx \int dy \{ N_{X(0)}\sigma^{(2)}_{n'-0}(\omega,\Phi)\Phi(x,y,z;\omega;t)^2$$
$$- 2N_{A(n')}\sigma^{(2)}_{n'-0}(\omega,\Phi)\Phi(x,y,z;\omega;t)^2$$
$$- N_{A(n')}\sigma^{(2)}_{\mathrm{ion}-n'}\Phi(x,y,z;\omega;t)^2 \}, \tag{5}$$

where $\sigma^{(2)}_{n'-0}(\omega,\Phi)$ is the intensity-dependent cross section for two-photon excitation from the $X\ ^2\Pi_{1/2}\ n''=0$ level to

the n'th level of the $A\ ^2\Sigma^+$ state and $\sigma^{(2)}_{\text{ion}-n'}$ is the cross section for two-photon ionization from $A\ ^2\Sigma^+\ n'$. In this work we neglect the contribution to the $A\ ^2\Sigma^+$ population arising from transitions out of the upper spin-orbit level of the $X\ ^2\Pi_r$ manifold, which is located within the bandwidth of 100-fs laser pulses, and also omit rotational effects.

The quantity $\sigma^{(2)}_{n'-0}(\omega,\Phi)$ is calculated at each coordinate in space time by

$$\sigma^{(2)}_{n'-0}(\omega,\Phi)=\sigma^{2,\text{res}}_{n'-0}\exp[-\xi\{\hbar(\omega-\omega_{\text{res}}(n'))-\chi U_p\}^2],\tag{6}$$

where $\sigma^{2,\text{res}}_{n'-0}$ is the resonant two-photon cross section in the weak-field limit and $\omega_{\text{res}}(n')$ is the resonant angular frequency of the two-photon absorption transition to the n'th vibrational level of the $A\ ^2\Sigma^+$ state. The factor ξ is calculated from the spectral width of the laser (e.g., FWHM of 1.8 nm at 400 nm) and χ is a fitting parameter that measures the magnitude of the ac Stark shift of the $3s\sigma$ Rydberg electron as a fraction of U_p. Based on the observed profiles, the spatiotemporal incident intensity distribution is taken to have the form

$$I(x,y,z;\omega;t)=\hbar\omega\Phi(x,y,z;\omega;t)$$
$$=\frac{\epsilon}{\sqrt{\pi^3/\alpha\beta\delta}}\exp[-\alpha x^2-\beta y^2-\gamma-\delta t^2],\tag{7}$$

where x and y are the coordinates perpendicular to the laser beam propagation direction z. Integration over x and y in Eqs. (4) and (5) ensures conservation of energy (photon flux) per unit time and, though not indicated explicitly, $\Phi(x,y,z;\omega;t)$ is integrated over the optical cycles contained within the pulse envelope function. The parameter ϵ used here is the total energy per pulse monitored experimentally. The coefficients appearing in the exponential term of Eq. (7) were determined at each second-harmonic wavelength from the beam profiles (α, β) and second-order cross correlation (δ). The parameter γ in the exponential term accounts for the independence of the the intensity of the focused laser beam along the propagation direction z over the short length at the center of the confocal range viewed by the light-imaging optics. Integration along the beam propagation direction is taken into account by scaling the calculated fluorescence output from the model to the experimentally measured fluorescence signal.

Where possible, literature values were adopted for the cross sections required to solve Eqs. (4)–(6). The cross sections $\sigma^{(2)}_{\text{ion}-n'}$ for two-photon ionization from different n' levels of the $A\ ^2\Sigma^+$ state were estimated from the corresponding one-photon cross sections $\sigma^{(1)}_{\text{ion}-n'}$ via the ratio of their susceptibilities as [29]

$$\frac{\sigma^{(2)}_{\text{ion}-n'}}{\sigma^{(1)}_{\text{ion}-n'}}\simeq 10^{-34}.\tag{8}$$

For $\sigma^{(1)}_{\text{ion}-2}=6.0\pm1.0\times10^{-19}$ cm^2 [30], this gives $\sigma^{(2)}_{\text{ion}-2}\simeq6\times10^{-53}$ cm^4 s. Zacharias et al. found that $\sigma^{(1)}_{\text{ion}-n'}$ varied by only a factor of 1.4 for $n'=0-2$, with the largest value observed for $n'=1$ [30]. Within the bounds of the present, simplified kinetic treatment, where the ionization potential increases linearly with intensity by an amount equivalent to the electronic ponderomotive energy (Fig. 2), it was assumed that for input into Eq. (5), $\sigma^{(2)}_{\text{ion}-n'}$ does not vary with wavelength across the range 395–415 nm, and has the value for ionization from $A\ ^2\Sigma^+\ n'=2$ determined from Eq. (8).

The ratio given by Eq. (8) appears to operate successfully for the $A\ ^2\Sigma^+\ n'=2\leftarrow X\ ^2\Pi_r\ n''=0$ transition of the neutral state, for which the one-photon cross section $\sigma^{(1,\text{res})}_{2-0}=6.5\times10^{-16}$ cm^2 determined from the absolute integrated absorption intensities reported by Bethke [31] is 10^{34} times larger than a recent measurement of the two-photon cross section of $\sigma^{(2,\text{res})}_{2-0}=2.2\times10^{-50}$ cm^4 s [32]. The oscillator strengths for the vibrationally resolved $A\ ^2\Sigma^+\ n'=2\leftarrow X\ ^2\Pi_r\ n''=0$ transitions derived from absolute intensity measurements [31,33] vary by a factor of 2 for $n'=0$, 1, and 2. Consequently, as for the two-photon $X\ ^1\Sigma^+\leftarrow A\ ^2\Sigma^+$ ionization cross section discussed above, it was again assumed that $\sigma^{(2,\text{res})}_{n'-0}$ is independent of the vibrational resonance n' in the $A\ ^2\Sigma^+$ state; i.e., that $\sigma^{(2,\text{res})}_{n'-0}=\sigma^{(2,\text{res})}_{2-0}$ for $n'=0-2$. To test the validity of these assumptions, we varied $\sigma^{(2,\text{res})}_{2-0}$ and $\sigma^{(2)}_{\text{ion}-n'}$ by one order of magnitude on either side of the above estimates, finding very little effect on the calculated dependence of fluorescence yield as a function of laser intensity.

We note the results of the theoretical investigation of Cremaschi, who determined values of $\sigma^{(2,\text{res})}_{2-0}=2.9\times10^{-52}$ cm^4 s for two-photon absorption and $\sigma^{(2)}_{\text{ion}-2}=8.8\times10^{-47}$ cm^4 s for two-photon ionization from time-dependent perturbation theory and frozen-core self-consistent-field (SCF) calculations of the NO Rydberg states [34]. We find that using a value of $\sigma^{(2)}_{\text{ion}-n'}$ six orders of magnitude larger than that predicted by Eq. (8) results in zero fluorescence emission according to Eq. (9) for all incident laser intensities considered here, as all NO $A\ ^2\Sigma^+$ molecules are then $2+2$ ionized. For four-photon nonresonant NO$^+$ $X\ ^1\Sigma^+\leftarrow$NO $X\ ^2\Pi_r$, $n'=0$ ionization from the neutral ground state we adopt the value $\sigma^{(4)}_{\text{ion}-0}=7.1\pm0.1\times10^{-117}$ cm^8 s^3 determined by He and Becker for 532-nm laser light [25] rather than the result derived from perturbation theory applied to SCF Rydberg orbitals, which is some 19 orders of magnitude higher [34].

Clearly, the kinetic treatment of Eqs. (4) and (5) offers an incomplete picture of the intensity dependence of state shifting, neglecting as it does the nonperturbative excitations that dominate ionization processes at high intensities [5,35]. Even in the absence of multiphoton above-threshold (and dissociative) ionization at $I<10^{13}$ W cm^{-2}, $2+1$ ionization is energetically possible for the wavelengths of 395 and 400 nm used in this experiment, but the $\Delta n=0$ Franck-Condon expectation for ionizing transitions from NO Rydberg states ensures that $2+2$ ionization is overwhelmingly most probable. Stark shifting during the leading edge of intense laser pulses may facilitate resonantly enhanced ionization through

$2+1+1$ or $3+1$ photon absorptions via high-lying Rydberg states [36]. We suspect that such processes may be at least partially responsible for the inability of Eqs. (4) and (5) to predict correctly the fluorescence yield at $I \geqslant 2.5 \times 10^{13}$ W cm^{-2}. At intensities below about this value, Eqs. (4) and (5) predict that no population will remain in the $A\ ^2\Sigma^+$ state for long enough to fluoresce in the presence of additional, enhanced ionization routes: for this reason, extra processes contributing to $-dN_{A(n')}/dt$ are neglected in a simplified treatment of the data.

The coupled differential equations for the first three vibrational levels of the $A\ ^2\Sigma^+$ state are integrated over time and space to yield a final population in the $n'=2$ level, $N_{A(n')}^f$. This is taken to be directly proportional to the fluorescence signal S_F according to

$$S_F = \kappa N_{A(n')}^f. \qquad (9)$$

The parameter κ is a scaling factor used to normalize the measured electronic signal from the photomultiplier tube to the populations generated by Eqs. (4) and (5) and spatially averages the fluorescence imaged into the monochromator from the center of the confocal distance of the laser beam. To simulate the experiment, S_F is calculated for each incident laser intensity and wavelength.

IV. RESULTS AND DISCUSSION

Figure 3 shows graphs of $A\ ^2\Sigma^+\ n'=2 \rightarrow X\ ^2\Pi_r\ n''=0$ fluorescence intensity plotted as a function of incident laser intensity for two-photon wavelengths of 410, 405, and 400 nm. The other two-photon wavelengths studied, 415 and 395 nm, produced no significant $A\ ^2\Sigma^+\ n'=2 \rightarrow X\ ^2\Pi_r\ n''=0$ fluorescence at 205 nm. At the ''resonant'' wavelength, 410 nm, Fig. 3(a) reveals that S_F increases quadratically, with a peak intensity at $I \leqslant 1 \times 10^{13}$ W cm^{-2}, and then rapidly saturates. This effect is interpreted as an ac Stark shift of the $A\ ^2\Sigma^+\ n'=2$ level to higher energies as the peak laser intensity is increased. In this way the two-photon energy becomes nonresonant, and an increase in intensity does not bring about further population of the $n'=2$ level. Figure 3(b) indicates that the amount of fluorescence observed after irradiation by a 405-nm laser light is small up to $I<1 \times 10^{13}$ W cm^{-2}, at which point the intense radiation begins to populate the $n'=2\ A\ ^2\Sigma^+$ level. For a 400-nm incident light, a further increase of peak intensity to $I \approx 1.5 \times 10^{13}$ W cm^{-2} is required before the $A\ ^2\Sigma^+\ n'=2$ state is tuned into resonance. At $\lambda=395$ nm, no fluorescence is observed because the Stark shift required to tune the $n'=2$ level into resonance could not be achieved for $I \leqslant 6 \times 10^{13}$ W cm^{-2}. In the absence of negative Stark shifts, no $A\ ^2\Sigma^+ \rightarrow X\ ^2\Pi_r$ fluorescence was observed at wavelengths such as 415 nm, longer than the zero-field resonance at 410 nm.

The two parameters not fixed in the model are χ and κ [Eqs. (6) and (9)]. The factor χ scales the ac Stark shift from $0(\chi=0)$ to $U_p(\chi=1)$; when $\chi=1$, the shift is that expected for a free electron. The factor κ scales the calculated populations to the measured fluorescence intensities. For each
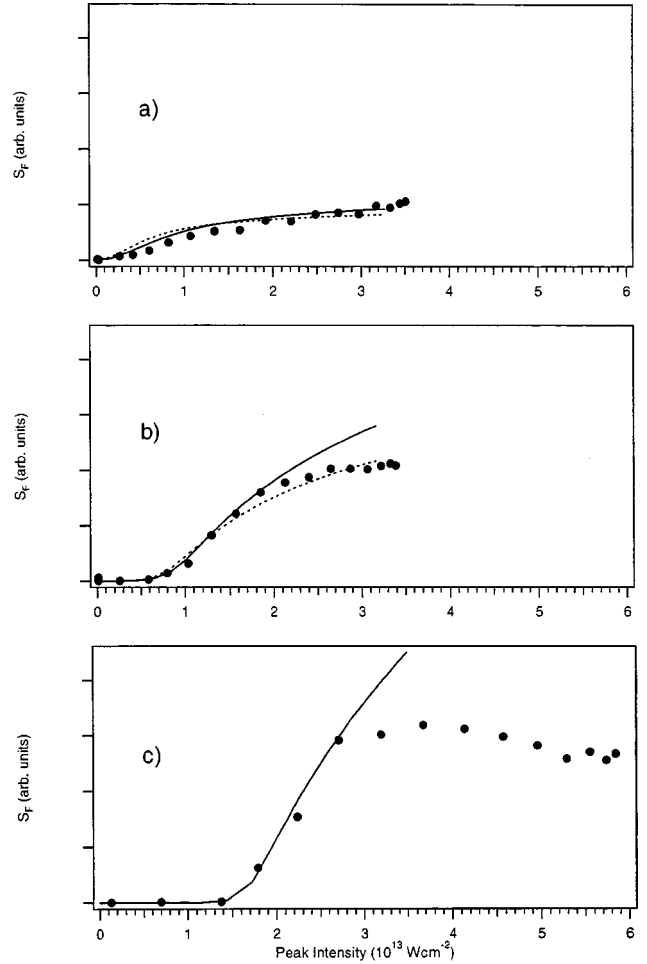

FIG. 3. Graphs of the intensity of $A\ ^2\Sigma^+\ n'=2 \rightarrow X\ ^2\Pi_r\ n''=0$ fluorescence S_F versus incident laser intensity calculated using Eq. (9) at different two-photon $A\ ^2\Sigma^+ \leftarrow X\ ^2\Pi_r$ excitation wavelengths: (a) 410 nm; (b) 405 nm; (c) 400 nm. The solid lines in all three diagrams indicate optimized nonlinear least-squares fits to the data according to Eqs. (4) and (5), while the dashed lines in diagrams (a) and (b) indicate fits obtained with χ fixed at 0.40, the optimum value derived from diagram (c). Dark circles represent the experimental points.

wavelength studied, the factors χ and κ are expected to be the same. To test this conjecture, each curve was fitted individually. It was found that a best fit to the data recorded at 410 nm was obtained with values of $\chi=0.26$ and $\kappa=0.53$, and it is displayed as a solid line in Fig. 3(a). The optimum fit to the 405 and 400-nm data shown in Figs. 3(b) and 3(c), also indicated by solid lines, required values of $\chi=0.32$ and $\kappa=1.20$, respectively, and $\chi=0.40$ and $\kappa=8.80$. For 400 nm, Eqs. (4) and (5) generated the poorest fit to the data. The fact that the intensity dependence of the $A\ ^2\Sigma^+\ n'=2 \rightarrow X\ ^2\Pi_r\ n''=0$ fluorescence at different wavelengths is best fitted with different κ values reveals, as might be anticipated, that the kinetic scheme of Eqs. (4)–(9) represents an imperfect description of the phenomenon.

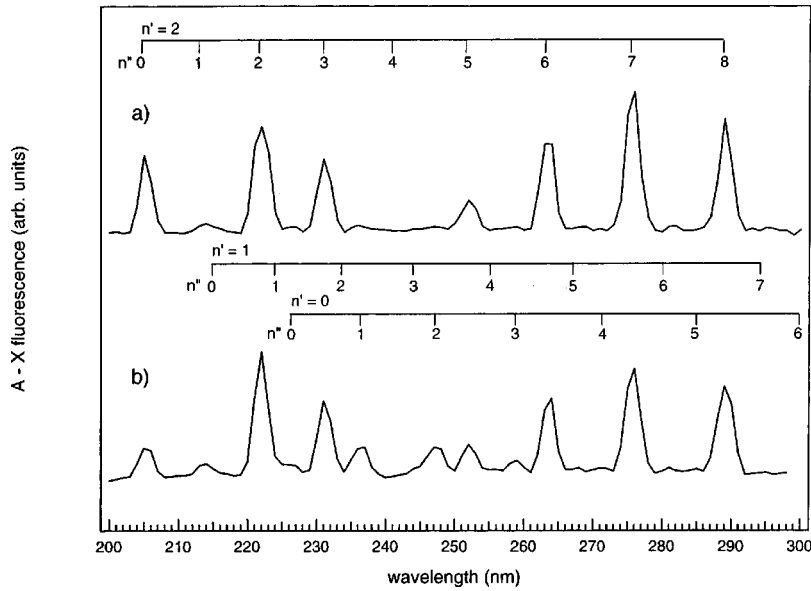The experimental variation of S_F with laser intensity could not be reproduced by the kinetic model for intensities

FIG. 4. NO $A\ ^2\Sigma^+ \to X\ ^2\Pi_r$ dispersed fluorescence spectra recorded with a spectral resolution of 1 nm: (a) $n'=2 \to n''$ spectrum resulting from resonant two-photon $A\ ^2\Sigma^+\ n'=2 \leftarrow X\ ^2\Pi_r\ n''=0$ absorption at $\lambda=410$ nm and $I=3\times10^{12}$ W cm^{-2}; (b) $n'=2,\ 1,\ 0 \to n''$ spectrum resulting from nonresonant $A\ ^2\Sigma^+ \leftarrow X\ ^2\Pi_r$ two-photon absorption at $\lambda=400$ nm and $I=6\times10^{13}$ W cm^{-2}.

greater than about 2.5×10^{13} W cm^{-2}. Saturation of the ionization rate at 532 nm at similar intensities [25] would imply that at $I>2.5\times10^{13}$ W cm^{-2}, the peak intensity of the pulse completely depletes the ground state of the NO molecules at the center of the focal volume of the laser. Population of the $A\ ^2\Sigma^+$ state is then no longer possible with increasing peak intensity and hence no further increase in fluorescence should be monitored. In our experiments, we suspect that fluorescence observed at $I\geqslant2.5\times10^{13}$ W cm^{-2} most likely originates from molecules located within concentric shells of decreasing intensity about the center of the laser beam in the transverse dimension, where Stark-induced population of the $A\ ^2\Sigma^+\ n'=2$ level can still occur. Stimulated emission processes, which would increase the light intensity along the laser propagation axis at the expense of transverse emission, only occur during an intense laser pulse, and so are able to suppress $A\ ^2\Sigma^+ \to X\ ^2\Pi_r$ fluorescence observed perpendicular to the beam direction over the 202-ns [27] radiative lifetime of the $A\ ^2\Sigma^+$ state by a factor on the order of 10^{-4}. As discussed in Sec. III, the breakdown of a simple kinetic treatment of the time-dependent Rydberg state population in this intensity regime may be interpreted as being due to the onset of processes such as above threshold and tunnel ionization and dissociation, which are known to dominate nonperturbative laser-molecule interactions [1,3,4,15,35].

Fitting the data of Figs. 3(a) and 3(b) for 410 and 405-nm excitation with a common value of χ, shown as dashed lines, yields an optimal result of $\chi=0.40$, consistent with the best fit to the 400-nm data shown as a solid line in Fig. 3(c). However, in this case the calculated fluorescence signal at 400 nm needed to be scaled ten times bigger than S_F at 405 and 410 nm to agree with experiment. The successful aspect of the kinetic model is that it can quantitatively reproduce the shapes of the fluorescence curves at intensities below $2-3\times10^{13}$ W cm^{-2} for a common value of χ at all wavelengths. The very nature of a model adapted from a perturbative treatment means, of course, that it is bound to fail at high intensities, for which an electronic wave-packet descrip-

tion of the $3s\sigma$ electron would provide a better description of the phenomenon [37].

An intuitive and useful observation is that the point of inflection (POI) of each of the curves of Fig. 3 lies very near that for which the peak intensity of the laser pulse has shifted the state of interest ($A\ ^2\Sigma^+\ n'=2$) into resonance with the two-photon energy. The wavelengths that are resonant or nearly resonant at low intensities are obviously an exception. If we take the POI of the 400-nm curve [Fig. 3(c)] to be near 2×10^{13} W cm^{-2} and that for the 405-nm curve [Fig. 3(b)] to be near 1×10^{13} W cm^{-2}, then these intensities are in agreement with an ac Stark shift of $0.4U_p$. The POI predicted by Eqs. (4) and (5) is the most robust feature of the kinetic model, being resilient to large changes in the NO$^+$ $X\ ^1\Sigma^+$ $\leftarrow$ NO $A\ ^2\Sigma^+$, $n'=2$ two-photon ionization cross section and laser spectral width. It is suggested that this feature of the experimental curves can be used to provide a convenient estimate of χ.

The dispersed fluorescence spectrum recorded using high intensity 400-nm light reveals a number of features arising from NO $A\ ^2\Sigma^+\ n'=1$ and $n'=0$, and is displayed in Fig. 4. For a peak intensity of 6×10^{13} W cm^{-2} at this wavelength, a full ponderomotive shift would have a value of 0.89 eV. For the $A\ ^2\Sigma^+\ n'=0 \leftarrow X\ ^2\Pi_r\ n''=0$ resonance at 226 nm to shift to 200 nm (two photons at 400 nm), an ac Stark shift of 0.72 eV is required, commensurate with a value of $\chi=0.81$. For two-photon $A\ ^2\Sigma^+ \leftarrow X\ ^2\Pi_r$ excitation at 400 nm, the fitted curve of Fig. 3(a) indicates that some fluorescence is detected at a lower intensity than at the POI due to shifting of the $n'=2$ resonance within the red wing of the finite spectral width of the laser pulse: the value of $\chi=0.81$ may then be an overestimate. On the other hand, the shift may be even larger than 0.72 eV. Spectra such as that shown in Fig. 4 are of little predictive value in estimating χ, except to indicate that χ must be at least 0.4.

In summary, the data of Fig. 3 point to a value for χ of 0.4, indicating for the promoted $3s\sigma$ electron of NO $A\ ^2\Sigma^+$ a significant deviation from the ponderomotive shift ex-

pected for a free electron. It is possible to conjecture that such a result is a manifestation of the still-dominant attractive Coulombic interaction experienced by an electron in the $A\ ^2\Sigma^+$ state. In contrast, ac Stark shifts of similar magnitude to the ponderomotive energy are expected for the occupation of high-lying Rydberg states situated close to the ionization potential, where the electron dynamics are more strongly influenced by the electric vector of the incident laser beam.

V. CONCLUSIONS

Through measurements of the NO $A\ ^2\Sigma^+\,n'=2 \rightarrow X\ ^2\Pi_r\,n''=0$ fluorescence yield as a function of incident laser intensity, it has been found that light at wavelengths to the blue of the $A\ ^2\Sigma^+\,n'=2\leftarrow X\ ^2\Pi_r\,n''=0$ two-photon absorption resonance in the low-field limit can result in population of the $n'=2$ vibrational level at ntensities $>2 \times 10^{13}\,\mathrm{W\,cm^{-2}}$. Fluorescence detection as a function of laser intensity possesses the advantage that the intensity-dependent population of the populated state is determined directly, and hence yields quantitative information on the magnitude of ac Stark effects. A kinetic model that takes into account the Stark shift of the $A\ ^2\Sigma^+$ state with incident laser intensity is able to predict that the variation of $A\ ^2\Sigma^+ \rightarrow X\ ^2\Pi_r$ fluorescence allows a quantitative estimate of the extent of the ac Stark shift of the $3s\sigma\ A\ ^2\Sigma^+$ electron as at least 0.4 of the full ponderomotive shift expected for a free electron. This value is intermediate between those for electrons in high-lying Rydberg states of atoms [7] and molecules [14,15], which experience essentially ponderomotive shifts, and those for electrons in valence states subject to stronger nuclear force fields. It was further found that the point of inflection of curves of fluorescence intensity versus incident laser intensity lies near the point where the peak intensity of the beam corresponds to a shift into resonance of the state in question. It would appear that despite the complex nature of the intense light-molecule interaction, ultrafast laser-induced fluorescence can be applied to determine the ac Stark effect of nonponderomotively shifted Rydberg states in strong laser fields.

[1] A. D. Bandrauk, *Molecules in Laser Fields* (Dekker, New York, 1993).

[2] M. H. Mittleman, *Theory of Laser-Atom Interactions* (Plenum, New York, 1982).

[3] P. Agostini and E. Mevel, in *Laser Interactions with Atoms, Solids, and Plasmas*, edited by R. M. More (Plenum, New York, 1994), pp. 11–38.

[4] P. Avan, C. Cohen-Tannoudji, J. Dupont-Roc, and C. Fabre, J. Phys. (Paris) **37**, 993 (1976); L. Pan, L. Armstrong, Jr., and J. H. Eberly, J. Opt. Soc. Am. B **3**, 1319 (1986); B. Dai and P. Lambropoulos, Phys. Rev. A **34**, 3954 (1986).

[5] R. R. Freeman and P. H. Bucksbaum, J. Phys. B **24**, 325 (1991).

[6] P. H. Bucksbaum, R. R. Freeman, M. Bashkanski, and T. J. McIlrath, J. Opt. Soc. Am. B **4**, 760 (1987), and other articles on multiphoton excitations in the same issue; J. H. Eberly, J. Javanainen, and K. Rzazewski, Phys. Rep. **204**, 331 (1991), and references therein.

[7] See, for example, T. R. O'Brian, J.-B. Kim, G. Lan, T. J. McIlrath, and T. B. Lucatorto, Phys. Rev. A **49**, R649 (1994), and references therein.

[8] H. Pummer, H. Egger, T. S. Luk, T. Srinivasan, and C. K. Rhodes, Phys. Rev. A **28**, 795 (1983); T. Srinivasan, H. Egger, T. S. Luk, H. Pummer, and C. K. Rhodes, IEEE J. Quantum Electron. **QE-19**, 1874 (1983); N. Bjerre, R. Kachru, and H. Helm, Phys. Rev. A **31**, 1206 (1985); D. W. Chandler and L. R. Thorne, J. Chem. Phys. **85**, 1733 (1986); M. J. J. Vrakking, A. S. Bracker, T. Suzuki, and Y. T. Lee, Rev. Sci. Instrum. **64**, 645 (1993).

[9] M. A. Quesada, A. M. F. Lau, D. H. Parker, and D. W. Chan-

dler, Phys. Rev. A **36**, 4107 (1987).

[10] B. Girard, N. Billy, J. Vigué, and J. C. Lehmann, Chem. Phys. Lett. **102**, 168 (1983); S. Xu, G. Sha, B. Jiang, W. Sun, X. Chen, and C. Zhang, J. Chem. Phys. **100**, 6122 (1994); S. Xu, G. H. Sha, J. B. He, and C. H. Zhang, *ibid.* **100**, 1866 (1994).

[11] B. Girard, G. O. Sitz, R. N. Zare, N. Billy, and J. Vigué, J. Chem. Phys. **97**, 26 (1992).

[12] M. D. Di Rosa and R. L. Farrow, J. Opt. Soc. Am. B **16**, 861 (1999).

[13] H. Stapelfeldt, H. Sakai, E. Constant, and P. B. Corkum, Phys. Rev. Lett. **79**, 2787 (1997).

[14] H. Rottke, J. Ludwig, and W. Sandner, J. Phys. B **30**, 2835 (1997); J. Ludwig, H. Rottke, and W. Sandner, Z. Phys. D: At., Mol. Clusters **42**, 57 (1997).

[15] M. Saeed, B. Yang, X. Tang, and L. F. DiMauro, Phys. Rev. Lett. **24**, 3519 (1992).

[16] S. Ganguly and K. Rai Dastidar, Phys. Rev. A **37**, 1363 (1988).

[17] H. Sakai and K. Miyazaki, Appl. Phys. B: Lasers Opt. **B61**, 493 (1995).

[18] G. N. Gibson, R. R. Freeman, and T. J. McIlrath, Phys. Rev. Lett. **67**, 1230 (1991).

[19] A. l'Huillier, L.-A. Lompré, D. Normand, X. Tang, and P. Lambropoulos, J. Opt. Soc. Am. B **6**, 1790 (1989).

[20] G. N. Gibson, R. R. Freeman, T. J. McIlrath, and H. G. Muller, Phys. Rev. A **49**, 3870 (1994).

[21] O. Faucher, E. Hertz, B. Lavorel, R. Chaux, T. Dreier, H. Beger, and D. Charalambidis, J. Phys. B **32**, 4485 (1999).

[22] W. M. Huo, K. P. Gross, and R. L. McKenzie, Phys. Rev. Lett. **54**, 1012 (1985).

[23] L. Deng, W. R. Garrett, and M. G. Payne, Chem. Phys. Lett. **271**, 15 (1997); S. T. Pratt, Phys. Rev. A **39**, 4877 (1989); W. R. Garrett, W. R. Ferrell, J. C. Miller, and M. G. Payne, *ibid.* **32**, 3790 (1985); M. G. Payne, J. Y. Zhang, and W. R. Garrett, *ibid.* **48**, 2334 (1993).

[24] P. Ludowise, M. Blackwell, and Y. Chen, Chem. Phys. Lett. **258**, 530 (1996).

[25] C. He and C. H. Becker, Phys. Rev. A **55**, 1300 (1997).

[26] K. P. Huber and G. Herzberg, *Molecular Spectra and Molecular Structure IV: Constants of Diatomic Molecules* (Van Nostrand Reinhold, New York, 1979), pp. 466–480.

[27] L. G. Piper and L. M. Cowles, J. Chem. Phys. **85**, 2419 (1986).

[28] See, for example, B. Witzel, N. A. Papadogiannis, C. J. G. J. Uiterwaal, H. Schröder, and D. Charalambidis, Phys. Rev. A **60**, 3311 (1999); B. Witzel, C. J. G. J. Uiterwaal, H. Schröder, D. Charalambidis, and K. L. Kompa, *ibid.* **58**, 3836 (1998).

[29] Y. R. Shen, *The Principles of Nonlinear Optics* (Wiley, New York, 1984), Chap. 18, pp. 334–335.

[30] H. Zacharias, F. de Rougemont, T. F. Heinz, and M. M. T. Loy, J. Chem. Phys. **105**, 111 (1996).

[31] C. W. Bethke, J. Chem. Phys. **31**, 662 (1959).

[32] K. Szczubliak, H. Adcock, C. Perkins, R. Stickrod, and M. P. McCann, J. Mol. Spectrosc. **169**, 590 (1995).

[33] D. Weber and S. S. Penner, J. Chem. Phys. **26**, 860 (1957).

[34] P. Cremaschi, J. Chem. Phys. **75**, 3944 (1981).

[35] A. Tablepour, S. Larochelle, and S. L. Chin, J. Phys. B **30**, 1927 (1997).

[36] J. A. Guest and L. C. Lee, J. Phys. B **14**, 3401 (1981).

[37] See, for example, N. Nurhuda and F. H. M. Faisal, Phys. Rev. A **60**, 3125 (1999); H. Yu, T. Zuo, and A. D. Bandrauk, *ibid.* **54**, 3290 (1996); S. Chelkowski, T. Zuo, O. Atabek, and A. D. Bandrauk, *ibid.* **52**, 2977 (1995).